Article

From Batch to Pilot: Scaling Up Arsenic Removal with an Fe-Mn-Based Nanocomposite

Jasmina Nikić , Jovana Jokić Govedarica , Malcolm Watson * , Đorđe Pejin , Aleksandra Tubić , Jasmina Agbaba

Posted Date: 23 June 2025

doi: 10.20944/preprints202506.1740.v1

Keywords: Arsenic removal; Fe-Mn nanocomposite; pilot scale; adsorption capacity; column tests

 doi:10.20944/preprints202506.1740.v1

Article

From Batch to Pilot: Scaling Up Arsenic Removal with an Fe-Mn-Based Nanocomposite

Jasmina Nikić, Jovana Jokić Govedarica, Malcolm Watson *, Đorđe Pejin, Aleksandra Tubić and Jasmina Agbaba

Department of Chemistry, Biochemistry and Environmental Protection, University of Novi Sad, Faculty of Sciences, Trg Dositeja Obradovića 3, 21000 Novi Sad, Serbia

* Correspondence: malcolm.watson@dh.uns.ac.rs

Abstract

Arsenic contamination in groundwater is a significant public health concern, with As(III) posing a greater and more challenging risk than As(V), due to its higher toxicity, mobility, and weaker adsorption affinity. Fe-Mn-based adsorbents offer a promising solution, simultaneously oxidizing As(III) to As(V), enhancing its adsorption. This study evaluates an Fe-Mn nanocomposite across typical batch (20 mg of adsorbent), fixed-bed column (28 g) and pilot-scale (2.5 kg) studies, bridging the gap between laboratory and real-world applications. Batch experiments yielded maximum adsorption capacities of 6.25 mg/g and 4.71 mg/g in synthetic and real groundwater respectively, demonstrating the impact of water matrix on adsorption. Operational constraints and competing anions lead to a lower capacity at the pilot (0.551 mg/g). Good agreement was obtained by the breakthrough curves at the pilot (breakthrough at 475 Bed Volumes) and the fixed-bed column studies (365–587 Bed Volumes) under similar empty bed contact times (EBCT). The Thomas, Adams-Bohart, and Yoon-Nelson models demonstrated that lower flow rates and extended EBCT significantly enhance arsenic removal efficiency, prolonging operational lifespan. Our findings demonstrate the necessity of continuous-flow experiments using real contaminated water sources, and the importance of optimising flow conditions, EBCT and pre-treatment, in order to successfully scale up Fe-Mn-based adsorbents for sustainable arsenic removal.

Keywords: Arsenic removal; Fe-Mn nanocomposite; pilot scale; adsorption capacity; column tests

1. Introduction

Arsenic contamination in groundwater poses significant challenges to public health and environmental safety, particularly in regions where geochemical and anthropogenic activities contribute to elevated arsenic levels [1–3]. Chronic exposure to arsenic, even at low concentrations, has been linked to severe health risks, including cancer, cardiovascular disease, and neurological disorders [4,5]. Consequently, the development of efficient, scalable, and sustainable technologies for arsenic removal is a critical area of research.

Among various treatment methods, adsorption has emerged as a highly effective and versatile approach for arsenic remediation due to its simplicity, cost-effectiveness, and adaptability to various operational conditions [6]. In particular, Fe-Mn-based adsorbents have garnered significant attention for their dual functionality, utilizing the high affinity of iron and manganese oxides for arsenic species [7–11]. The combined oxidation and adsorption capabilities of Fe-Mn-based materials make them highly efficient in removing both As(III) and As(V) from water, addressing a wide range of contamination scenarios [12].

The majority of studies on Fe-Mn-based adsorbents primarily focus on batch adsorption experiments, often neglecting their evaluation under continuous operational conditions. This is mainly due to the challenges associated with establishing dynamic flow systems compared to batch setups. While batch studies are essential for determining equilibrium and kinetic parameters, they

 doi:10.20944/preprints202506.1740.v1

fail to replicate the complexities of real-world systems. Moreover, the arsenic concentration ranges used in batch experiments are often unrealistic and do not reflect the concentrations typically found in natural water sources. This can be problematic as in general, there is a strong correlation between a initial contaminant concentration and the maximum adsorption capacity (q_{max}) obtained in batch studies, regardless of the material used (see Supplementary Material Figure S1). As a result, adsorbents demonstrate high adsorption capacities in batch experiments (Table 1), but in real-world applications, may face significant limitations in continuous-flow systems due to factors such as flow dynamics, competition from coexisting ions, and long-term stability issues [13,14]. To address this gap, it is crucial to conduct larger scale performance tests under continuous-flow conditions. Investigations such as column and pilot-scale studies are essential for assessing the practical viability of newly developed adsorbents in water treatment applications [15–17].

Table 1. Adsorption performance of Fe-Mn based adsorbents in batch system.

Fe-Mn based adsorbents	Initial As concentration (mg/l)	Water matrix	pH	Adsorption capacity in batch system (mg/g)		References
				As(III)	As(V)	
Fe–Mn binary oxide	1-200	Synthetic	5	69.8	133	[18]
Magnetite coated with FMBO	0.2-50	Synthetic	7.0	55.9	54.1	[19]
Diatomite coated with Fe–Mn binary oxide	0.05-20	Synthetic	7.0	1.68	-	[20]
Macroporous anion exchanger-supported Fe–Mn binary oxide	1-50	Synthetic water	7.0	44.9	13.17	[21]
Starch-FMBO	0-300	Synthetic		161	-	[22]
Gelatin-FMBO	0-300			141	-	[22]
CMC-FMBO	0-300			104	-	[22]
Nanoscale Fe-Mn binary oxides loaded on zeolite(NIMZ)	2-100	Synthetic	7.0	47	49	[23]
Biochar coated with FMBO	0.01-10	Synthetic	7.0	14.4	12.2	[24]
GAC-FeMn	0.01-1	Synthetic	7.0	2.30	2.87	[13]
Chitosan-FMBO	0-24	Synthetic	7.0	54.2	-	[25]
Chitosan-FeMn	0.1-1	Synthetic	7.0	3.91	3.89	[26]
PET-FMBO	0.1-1	Synthetic	7.0	8.74	13.3	[11]
PE-FMBO	0.1-1	Synthetic	7.0	5.29	5.37	[11]
Graphene oxide chitosan coated FMBO (Fe/Mn GOCS)	5-300	Synthetic	7.62	109	-	[9]
Fe/Mn-C Layered Double Hydroxide Composite	5-100	Synthetic	-	41.9	33.6	[27]
Iron-manganese binary oxide	1-100	Synthetic	7.0	134	-	[6])

 doi:10.20944/preprints202506.1740.v1

nanoparticles on nylon 6 fibre

Continuous-flow experiments provide valuable insights into the dynamic behaviour of adsorbents, allowing researchers to evaluate their performance under realistic operational conditions. Key parameters such as flow rate, breakthrough volume, bed height (amount of adsorbent), empty bed contact time (EBCT), pH, and competing ion effects must be analysed to optimize performance [28]. These studies also highlight factors such as adsorbent stability, regeneration potential and overall operational efficiency. Pilot-scale investigations further enhance this understanding by simulating near-industrial conditions, offering a comprehensive evaluation of adsorbent performance over extended periods. They help identify potential bottlenecks and optimize process parameters, ensuring consistent and reliable performance. By integrating continuous-flow column and pilot-scale experiments, researchers can bridge the gap between laboratory findings and real-world applications, ultimately contributing to the development of scalable, sustainable, and effective water treatment technologies for arsenic removal [29].

To the best of our knowledge, few studies have evaluated the potential of Fe-Mn-based adsorbents for arsenic removal, particularly As(III), under continuous-flow conditions [9,21,25,30,31]. Even fewer have examined their performance under realistic operational conditions [13,32], highlighting the need for further research in continuous treatment systems to provide a more reliable assessment of the suitability of Fe-Mn-based adsorbents for scalable and sustainable arsenic removal solutions. This study aims to bridge the gap between theoretical and practical adsorption capacities by integrating batch, column, and pilot-scale experiments to assess a Fe-Mn nanocomposite under realistic operational scenarios. Comparative analyses across different experimental scales were conducted to evaluate adsorption efficiency and operational feasibility in real groundwater treatment conditions. Batch adsorption experiments were modelled using the Freundlich and Langmuir isotherms to describe equilibrium behaviour and adsorption capacity, providing initial insights into arsenic affinity under controlled conditions. To assess adsorbent performance under dynamic conditions, continuous-flow column and pilot-scale experiments were conducted using real arsenic-contaminated groundwater. Breakthrough curves were modelled using the Thomas, Adams-Bohart, and Yoon-Nelson models, enabling the prediction of adsorption performance, breakthrough time, and bed saturation under real operational conditions. These models provided a deeper understanding of the influence of flow rate, empty bed contact time (EBCT), and competitive adsorption effects from naturally occurring anions such as phosphate. Overall, these findings highlight the necessity of continuous-flow studies in adsorption research to ensure a more reliable evaluation of Fe-Mn-based adsorbents for large-scale water treatment applications.

2. Materials and Methods

2.1. Materials

The Fe-Mn nanocomposite adsorbent used in this study was developed for arsenic removal from groundwater. It is designed to oxidize As(III) and adsorb As(V), making it highly effective for water treatment applications. The material consists of iron and manganese oxides incorporated within a polymeric matrix, providing both mechanical stability and enhanced adsorption capacity. This combination allows for efficient contaminant removal while ensuring material durability and reusability. More exact details regarding the scaled up synthesis process and material characterization cannot be disclosed as they are subject to an intellectual property agreement. However, the adsorbent was tested for its performance in batch, column, and pilot-scale experiments to assess its arsenic removal efficiency under various conditions.

2.1. Investigated Water Matrices

 doi:10.20944/preprints202506.1740.v1

Batch and column experiments were conducted using both arsenic-contaminated groundwater and tap water spiked with As(III), whereas the pilot study exclusively used arsenic-contaminated groundwater. As explained below, the groundwater was also subject to aeration and sand filtration, to yield a third water matrix, aerated groundwater. The characteristics of the investigated water matrices are summarized in Table 2.

Table 2. Characteristics of the investigated water matrices.

Parameter	Water		
	Groundwater	Aerated groundwater	Spiked tap water
pH	7.73 ±0.05	7.81 ± 0.05	7.51±0.04
Conductivity(µS/cm)	514 ± 43	466 ± 12	490 ± 22
Turbidity (NTU)	1.55 ± 0.29	0.70 ± 0.05	0.31 ±0.07
TOC (mg/L)	1.38 ±0.10	1.53 ± 0.05	1.460 ± 0.05
Arsenic (µg/L)	115 ±6.4	90.0 ± 18.7	172 ± 20
Iron (µg/L)	395 ±28.1	5.36 ± 3.55	26.04 ± 2.20
Manganese (µg/L)	54 ±4.67	6.35 ± 8.52	3.22 ± 4.10
Ammonium (mg N/L)	0.44 ± 0.09	0.228 ± 0.12	0.454 ± 0.01
Nitrate (mg N/L)	1.57 ± 0.14	0.67 ± 0.11	0.05 ± 0.01
Orthophosphate (mg PO_4/L)	0.323 ± 0.11	0.075 ± 0.02	0.024 ± 0.01
Chloride (mg Cl/L)	3.77 ±3.19	0.673.19	27.25 ± 0.01

The groundwater sample exhibited a pH of 7.73 ± 0.05, indicating a slightly alkaline nature. The conductivity value of 514 ± 43 µS/cm suggests a moderate level of dissolved ions, likely originating from both geogenic sources and possible anthropogenic inputs. The relatively low turbidity (1.55 ± 0.29 NTU) indicates minimal suspended solids, implying that the groundwater is primarily affected by dissolved contaminants rather than particulate matter. Arsenic was detected at 115 ± 6.40 µg/L, significantly exceeding the WHO drinking water limit of 10 µg/L. This elevated concentration is attributed to geogenic sources, particularly the dissolution of arsenic-bearing minerals within the aquifer. Arsenic speciation analysis confirmed that As(III) is the dominant species (>90%), which aligns with the mildly reducing conditions of the water. Under these conditions, arsenic remains more mobile and difficult to remove compared to As(V), which is typically present in oxidizing environments and exhibits a stronger affinity for adsorbent surfaces. The presence of iron (0.395 ± 0.03 mg/L) and manganese (0.054 ± 0.005 mg/L) further supports this hypothesis, as both elements play a crucial role in arsenic mobilization through redox transformations. Under reducing conditions, Fe(III) and Mn(IV) can be reduced to Fe(II) and Mn(II), leading to arsenic desorption and increased mobility in groundwater. The Total Organic Carbon (TOC) concentration of 1.38 ± 0.10 mg/L indicates a moderate level of organic matter, which can influence arsenic mobility. Organic matter may enhance arsenic solubility by forming organo-arsenic complexes or facilitate its removal through interactions with Fe/Mn oxides. The nitrate concentration (1.57 ± 0.14 mg N/L) is well below the WHO guideline of 50 mg/L, indicating minimal agricultural or industrial contamination. However, ammonium (0.44 ± 0.09 mg N/L) and orthophosphate (0.323 ± 0.11 mg PO4/L) were detected at measurable levels, suggesting microbial activity or anthropogenic inputs. Phosphate is a known competitor with arsenic for adsorption sites, which may reduce the efficiency of adsorbent-based arsenic removal processes.

In order to avoid clogging of the adsorbent surface with ferric hydroxide floccs, aerated groundwater was also investigated. The original groundwater was aerated for 1 h and passed through a sand filter column to remove the resulting ferric hydroxide floccs. After filtration, 98.6% of the iron was removed. During this process, 21.7% of the arsenic was also removed by co-precipitation. A significant 77% reduction in the phosphate concentration in the aerated water was also observed.

 doi:10.20944/preprints202506.1740.v1

2.3. Batch Adsorption Experiment

Batch adsorption experiments were conducted to evaluate the adsorption capacity of the Fe-Mn nanocomposite under equilibrium conditions. Sorption isotherms were performed by spiking two different water matrices: groundwater naturally contaminated with arsenic and tap water. For each experiment, 20 mg of the sorbent was added to 40 mL glass vials containing 20 mL of the respective water matrix, with As(III) concentrations spiked to range from 0.1 mg/L to 10 mg/L. The samples were placed on a shaker at 180 rpm for 24 hours to ensure equilibration. After the equilibration period, the supernatant was decanted and preserved with concentrated HNO_3 before analysis. The concentrations of arsenic, iron, and manganese were determined by ICP/MS. The adsorption capacity at equilibrium was calculated based on the difference between the initial and final arsenic concentrations. All experiments were conducted in triplicate, with error bars representing standard deviations. To account for potential analytical errors and losses, control samples (without sorbent) were prepared under identical conditions for each water matrix. The arsenic concentrations in these control samples were used as reference initial concentrations for each experimental series.

The data obtained from these studies were modelled using the Freundlich and Langmuir isotherm models (Table 3) to determine the adsorption capacity, adsorption mechanism, and equilibrium parameters, which are critical for designing large-scale treatment systems

Table 3. Isotherm models used for fitting the adsorption data obtained for arsenic adsorption in batch systems.

Model	Equation	Parameters
Freundlich	$q_e = K_F C_e^{n_F}$	q_e - Adsorbed amount at equilibrium (mg/g), C_e-Equilibrium concentration (mg/L), K_F- Freundlich adsorption constant [(mg/g)(L/mg)^(1/n)]
Langmuir	$q_e = \frac{K_L C_L}{1 + \alpha_L C_e}$	q_e-Adsorbed amount at equilibrium (mg/g), C_e: Equilibrium concentration (mg/L), q_{max}: Maximum adsorption capacity (mg/g), K_L: Langmuir constant (L/mg)

2.4. Column Adsorption Experiment

The continuous fixed-bed adsorption studies were conducted in glass columns with an internal diameter of 2 cm. A 0.5 cm-thick layer of glass wool was placed at the bottom of the column to prevent adsorbent loss. The Fe-Mn nanocomposite was packed into the column in a predetermined quantity. Tap water spiked with As(III) to an initial concentration of 200 µg/L, or real groundwater contaminated with arsenic (with and without pretreatment via aeration), was pumped in a downflow mode at a constant flow rate using a peristaltic pump. To investigate the performance of the Fe-Mn nanocomposite in a fixed-bed adsorption column, experiments were conducted under various operational conditions (Table S1). The study included four different column setups, treating either tap water spiked with As(III), untreated groundwater, or aerated groundwater.

Column I and Column II (60 cm length, 2 cm internal diameter) were used for tap water spiked with As(III), both containing 131 mL of filter media with a bed depth of 41.7 cm. They were operated at different filtration and flow rates. Column I had a filtration rate of 1 m/h and an empty bed contact time (EBCT) of 25 minutes, whereas Column II had a higher filtration rate of 5 m/h and an EBCT of 5 minutes, allowing a comparison of adsorption efficiency under different flow conditions. Column III and Column IV (30 cm length, 2 cm internal diameter) were tested using natural groundwater and aerated groundwater, respectively. Both contained 62.8 mL of filter media with a bed depth of 20 cm, filtration rates of 01 m/h, and an EBCTs of 12 minutes. The comparison between these two columns aimed to assess the influence of aeration on arsenic removal efficiency, as aeration can affect the oxidation state of arsenic and enhance adsorption performance.

 doi:10.20944/preprints202506.1740.v1

The adsorption data collected from these experiments were further analysed using mathematical models, including the Thomas, Adams-Bohart, and Yoon-Nelson models, to characterize adsorption behaviour and predict breakthrough curves under continuous flow conditions. Both the linear and nonlinear forms of these models are summarized in Table 4. In this study, adsorption data were fitted using the nonlinear forms of these models.

Table 4. Column adsorption models used for fitting adsorption data from column and pilot studies.

Models	Equation	Parameters
Thomas	$\frac{c_t}{c_0} = \frac{1}{1} + \exp\left(k_{Th} q_0 \frac{m}{Q} - c_0 t\right)$	c_t: Concentration at time (mg/L), c_0: Initial concentration (mg/L), k_{Th}: Thomas rate constant (L/min·mg), q_0: Maximum adsorption capacity (mg/g), m: Mass of adsorbent (g), Q: Flow rate (L/min), t: Time (min)
Adams-Bohart	$\frac{c_t}{c_0} = \exp\left(k_{AB} c_0 t - k_{AB} N_0 \frac{L}{u}\right)$	c_t: Concentration at time (mg/L), c_0: Initial concentration (mg/L), k_{AB}: Adams-Bohart rate constant (L/mg·min), N_0: Saturated adsorption capacity (mg/L), L: Packed bed length (cm), t: Time (min), u: Linear velocity (cm/min)
Yoon-Nelson	$\frac{c_t}{c_0} = \frac{1}{1} + \mathrm{e}\, KYN(\tau - t)$	ct: Concentration at time (mg/L), c_0: Initial concentration (mg/L), k_{YN}: Yoon-Nelson rate constant (L/min), τ: Time required for 50% breakthrough (min), t: Time (min)

2.5. Pilot Experiment

Following the batch and column experiments, a pilot-scale study was conducted using a continuous-flow filtration unit to assess the efficiency of Fe-Mn polymer nanocomposite for arsenic removal under real-world conditions. The system was installed on site at a waterworks with arsenic-contaminated groundwater. The filtration unit consisted of a pressure vessel column (20.3 cm in diameter, 43 cm in height) with a total volume of 10 L, filled with Fe-Mn polymer nanocomposite adsorbent. The unit was fed arsenic-contaminated groundwater by a peripheral pump and included flowmeters, pressure gauges, sampling taps for water quality monitoring and a backwash system utilising treated water. The unit was run continuously with groundwater containing elevated As(III) levels, allowing for performance assessment under varying operational conditions (Table 5). Arsenic removal efficiency was determined by comparing influent and effluent concentrations by ICP-MS analysis. The effects of flow rate, EBCT, and bed depth on treatment performance were examined through modelling using the Thomas, Adams-Bohart, and Yoon-Nelson models (Table 4), while breakthrough curves were generated to assess media longevity and optimize replacement cycles.

Table 5. Operational condition at pilot filtration unit with Fe-Mn nanocomposite adsorbent.

	Filter media volume (L)	Mass of media (kg)	Bed depth (m)	Filtration rate (m/h)	EBCT (min)	Flow rate Q (L/h)
Pilot A	3.5	1.6	0.11	1.25	5.12	40
Pilot B	5.5	2.5	0.17	0.62	16.5	22

 doi:10.20944/preprints202506.1740.v1

2.6. Analytical Methods

The pH of the samples was measured using a METTLER TOLEDO FiveEasy Plus pH meter FP20-Std-Kit. The electrical conductivity of the groundwater and tap water was determined using a WTW Cond 3110 conductometer, following the SRPS EN 27888:2009 method. Turbidity was measured using a Thermo Scientific Eutech TN-100 turbidimeter. The total organic carbon (TOC) content in the water was determined using the Elementar Vario TOC Select instrument, according to the SRPS ISO 8245:2007 method. The orthophosphate content was determined spectrophotometrically with ammonium molybdate, following the SRPS EN ISO 6878:2008 method. The nitrate content was analysed spectrophotometrically with sulfosalicylic acid, according to the SRPS ISO 7890-3:1998 method. The chloride content was determined titrimetrically using silver nitrate with a chromate indicator (Mohr's method), following the SRPS ISO 9297/1:2007 method. Ammonium concentration in water was determined spectrophotometrically using the SRPS H.Z1.184:1974 method. The arsenic, iron, and manganese content in the water samples was determined using inductively coupled plasma mass spectrometry (ICP-MS) with a mass detector (Agilent Technologies 7700 Series ICP-MS), following US EPA method 6020B. The method detection limit (MDL) for arsenic, iron, and manganese was 0.001 mg/L.

3. Results and Discussion

3.1. Batch Adsorption Study

The adsorption affinity of the FMBO nanocomposite for arsenic was evaluated through batch experiments conducted under equilibrium conditions, using two different water matrices: tap water spiked with As(III) and arsenic-contaminated groundwater (Figure 1). The experimental data obtained were further analysed using the two most commonly applied isotherm models, Freundlich and Langmuir, to determine key adsorption parameters such as adsorption capacity and intensity. The corresponding parameters of the applied models are summarized in Table 6.

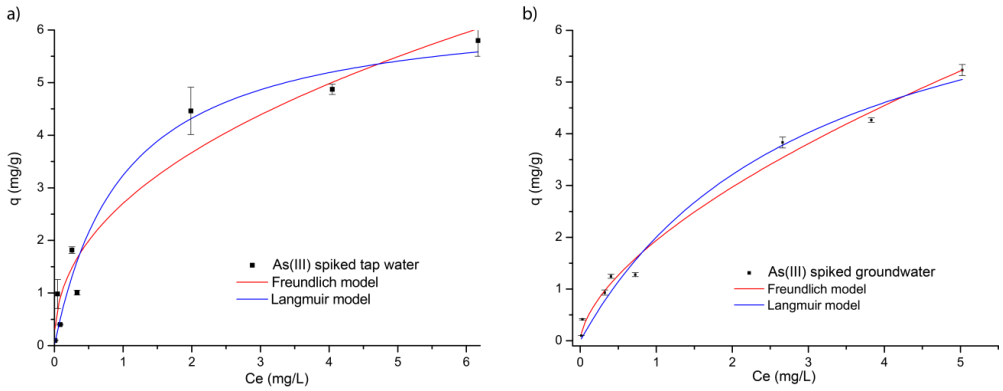

Figure 1. Freundlich and Langmuir adsorption isotherms of arsenic adsorption on FMBO nanocomposite a) Tap water spiked with As(III) and b) spiked groundwater (C_0 = 0.1–10 mg/L, pH = 7.02 ± 0.2).

Table 6. Parameters of Freundlich and Langmuir isotherm models for arsenic adsorption on FMBO nanocomposite.

	Freundlich model			Langmuir model		
Matrix type	**n**	**K_F (mg/g)/(mg/L)^n**	**R^2**	**q_{max} (mg/g)**	**K_L (L/mg)**	**R^2**
As(III) spiked tap water	0.640	2.70	0.9459	6.25	0.992	0.9577
As(III) spiked groundwater	0.420	1.79	0.9349	4.63	0.343	0.9452

 doi:10.20944/preprints202506.1740.v1

Based on the coefficient of determination (R^2) values, both models showed a strong correlation with the experimental data ($R^2 > 0.93$). However, the Langmuir model shower a better agreement with the experimental data ($R^2 > 0.94$). The Freundlich model, which describes multilayer adsorption on a heterogeneous surface, indicated that adsorption was more favourable in spiked tap water (n = 0.640) than in real groundwater (n = 0.420), as expected. The higher value of Freundlich constant (K_F = 2.70 mg/g (mg/L)^n) in spiked water compared to 2.13 mg/g (mg/L)^n in groundwater suggests that arsenic adsorption was more efficient in the cleaner tap water matrix. In the real groundwater, the presence of competing anions, primarily phosphate, reduced the number of adsorption sites available for arsenic. The Langmuir model, which assumes monolayer adsorption on a homogeneous surface, showed a higher theoretical maximum adsorption capacity (q_{max}) in spiked tap water (6.25 mg/g) compared to groundwater (4.63 mg/g), which is in agreement with Freundlich K_F values. Additionally, the Langmuir binding affinity constant (K_L) was significantly higher in spiked tap water (0.992 L/mg) than in groundwater (0.343 L/mg), indicating stronger arsenic binding in controlled conditions. The lower K_L value in groundwater confirms that arsenic adsorption is less efficient due to competition with naturally occurring ions.

3.2. Column Adsorption Study

After the batch adsorption experiments, we further investigated the performance of the Fe-Mn nanocomposite for arsenic removal through column experiments, ensuring a comprehensive evaluation of its effectiveness under continuous operational conditions. Arsenic removal by Fe-Mn nanocomposite was evaluated under four distinct conditions. In Columns I and II, tap water spiked with As(III) was passed through the column at different flow rates (5.2 mL/min and 26.2 mL/min), corresponding to empty bed contact times (EBCT) of 25 minutes and 5 minutes, respectively. In Columns III and IV, real groundwater containing arsenic—both with and without aeration—was used as the feed solution, with both columns operating at a constant flow rate of 5.2 mL/min (Table S1, supplementary material). The breakthrough curves illustrating arsenic removal under these different conditions are presented in **Figure 2**. Breakthrough curves as a standard method illustrate arsenic removal in continuous-flow column experiments, showing effluent concentration changes over time, whereby the breakthrough point was defined as the stage at which the arsenic concentration in the treated water exceeded the regulatory limit of 10 µg/L. In Figure 2, the breakthrough curves are depicted as C/C_0 vs. bed volume. Bed volume is the volume of water treated expressed as multiples of the adsorbent volume. The **initial arsenic concentration** in the tap water feed for **Columns I and II** was **172 ± 20 µg/L,** with the breakthrough point for total arsenic occurring at **10 µg/L**, corresponding to a **C/C_0 ratio of 0.058**. The **initial arsenic concentrations in the groundwater and aerated** groundwater were **120.3 ± 18.2 µg/L (C/C_0 ratio of 0.08) and 90 ± 12 µg/L (C/C_0 ratio of 0.11), respectively**.

 doi:10.20944/preprints202506.1740.v1

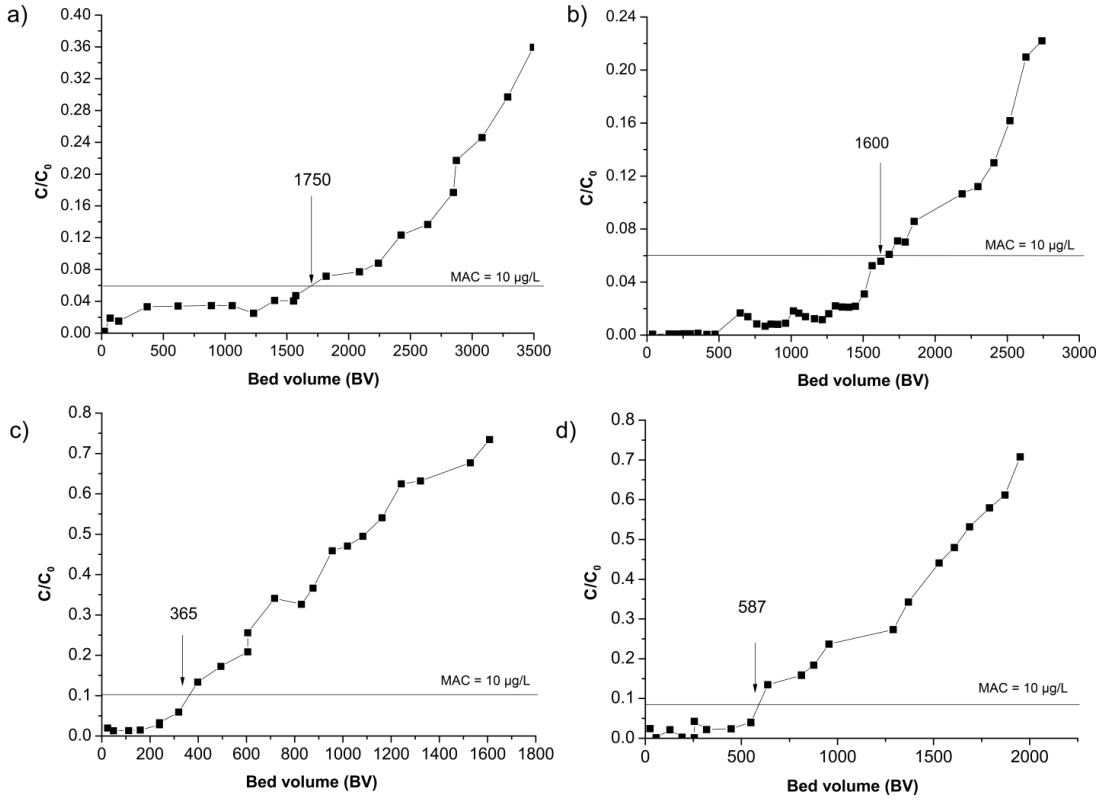

Figure 2. Breakthrough curves for arsenic removal using the Fe-Mn nanocomposite: a, b) Columns I and II: tap water spiked with As(III), c) aerated Column III and d) groundwater Column IV.

Based on the obtained results, the bed volumes (BV) treated before breakthrough varied significantly based on flow rate, empty bed contact time (EBCT), and water matrix composition. In Column I and Column II, where tap water spiked with As(III) was treated, arsenic breakthrough occurred after 1750 BV and 1600 BV, respectively (Figure 2a and 2b). A longer empty bed contact time (EBCT) of 25 minutes in Column I, compared to the shorter EBCT of 5 minutes in Column II, facilitated more effective arsenic removal. The extended contact duration allowed for improved interaction between the Fe-Mn nanocomposite and arsenic in solution, enhancing the adsorption process [20]. Similarly, Asif et al. [33] observed that increasing the flow rate led to a faster breakthrough, suggesting that at lower flow rates, the adsorbent takes more time to reach saturation. This phenomenon occurs because higher flow rates reduce the residence time of the adsorbate in the column, limiting its ability to interact with the adsorbent. In contrast, at lower flow rates, metal ions have more time to diffuse into the pores of the adsorbent, allowing for more effective adsorption via intra-particle diffusion. Conversely, for the higher flow rate, the arsenic solution will leave the column bed before the equilibrium can be reached.

In contrast, the real groundwater columns (III and IV) achieved significantly lower BV before breakthrough. In the aerated groundwater (Column III), breakthrough occurred at 365 BV, while in non-aerated groundwater (Column IV), breakthrough occurred at 587 BV (Figure 2c and d). Interestingly, aeration did not enhance arsenic removal efficiency as initially expected. Instead, it negatively impacted performance, despite iron concentrations decreasing significantly after aeration (from 395 µg/L to 5.36 µg/L). This reduction in iron likely diminished the co-precipitation effect, which otherwise could have aided arsenic removal. In contrast, non-aerated groundwater (Column 4) retained a higher iron concentration (395 µg/L), facilitating arsenic removal via co-precipitation and surface complexation with the Fe-Mn nanocomposites. Although Column IV exhibited slightly improved breakthrough performance (587 BV), overall arsenic removal remained much lower than in the tap water columns. This difference can be attributed to competing anions present in the groundwater, primarily phosphate (0.401 mg PO_4/L in groundwater), which likely inhibited arsenic

 doi:10.20944/preprints202506.1740.v1

adsorption by competing for active sites on the surface of the Fe-Mn nanocomposite [14]. Residual concentrations of Fe and Mn in water after treatment with the Fe-Mn nanocomposite were below the maximum allowable concentration of 0.3 mg/L and 0.05 mg/L, respectively confirming the stability of the Fe-Mn nanocomposite adsorbent (Table S2, supplementary material).

The performance of the Fe-Mn nanocomposite in fixed-bed column studies was further compared with other Fe-Mn-based adsorbents used in continuous-flow systems to evaluate its adsorption efficiency for As(III) and breakthrough volume (BV) under realistic conditions (Table 7). The Fe-Mn nanocomposite exhibited a breakthrough volume of 1700 BV in spiked tap water and 587 BV in non-aerated groundwater, demonstrating competitive performance compared to other Fe-Mn adsorbents, particularly in real groundwater conditions where adsorption efficiency is often hindered by competing ions.

 doi:10.20944/preprints202506.1740.v1

Table 7. Adsorption performance of Fe-Mn-based and similar adsorbents in continuous systems.

Fe-Mn based adsorbent	Length (cm)	Diameter (cm)	Mass of adsorbent (g)	Bed depth (cm)	Flow rate (mL/min)	EBCT (min)	Water matrix	BV before MAC breakthrough	Ref.
Graphene oxide chitosan coated FMBO (Fe/Mn GOCS)	3	1.6	7.67	-	1.5	-	Synthetic water matrix 10 or 50 mg/L As(III) pH 7	40 and 3	[9]
Macroporous anion exchanger-supported Fe–Mn binary oxide	13.0	1.2	-	-	-	3	Simulated water As(III) 100 µg/L; Nitrate 150 mg/L; Carbonate 200 mg/L; Chloride 300 mg/L; Sulphate 300 mg/L; pH 8.10	2300	[21]
Chitosan coated with Fe–Mn binary	32	1.9	30	25	-	10	Simulated groundwater As(III)/As(V) 233 µg/L; Nitrate 5 mg/L, Carbonate :159 mg/L; Silicate 12 mg/L; Phosphate 0.13 mg/L; pH 7.3	500 and 3200 for As(V) and As(III)	[25]
GAC-FMBO	80	1.7	-	30	6	12	Groundwater As(III): 120 µg/L; Conduct. 678 mS/cm; DOC 2.00mg/L; Alkalinity 7.68 mmol/L; Chloride 19.7mg/L; Carbonate 118 mg/L; Sulphate 15.7 mg SO4/L; Phosphate 1.33mg/L; Fe 35.4 µg/L Mn 21.5 µg/L; pH 8.22	83	[13]
HZO@D201 nanocomposite	13	1.2	5 ml	-	-	3	Simulated groundwater As(III) 0.1 mg/L; Magnesium 5 mg/L; Sulphate 50 mg/L; Calcium	600	[30]

 doi:10.20944/preprints202506.1740.v1

							15 mg/L; Silicate 5 mg/ L; Chloride 40 mg/L; Nitrate 8 mg/L; Carbonate 150 mg/L; pH : 8.2; Anaerobic groundwater; As_{tot} 0.0477 mg/L; As(III) 0.03 mg/L; Turbidity 0.7 NTU; Conductivity 530 mS/cm; TOC 2.84 mg/L; 305 mg/L;		
FMBO-diatomite	40	3	58	24	17	10	Magnesium 16 mg/L; Calcium 28 mg/L; Chloride 40 mg/L; Nitrate 9.8 mg/L; Phosphor 1.21 mg/L; Mn 0.15.1 mg/L; Fe 0.257 mg/L; Nitrogen 66 mg/L; pH: 7.4	7000 BVs after 15 regenerations	[20]
FMBO-diatomite	40	3	-	-	34	5	Spiked DI water with As(III)	4500	[32]
FMBO impregnated nylon 6 fibre (IMBNP-nylon 6)	4	1	-	-	-	0.65	Spiked RO water with As(III) 0.1 and 0.038 mg/L; Magnesium 5 mg/L; Sulphate 50 mg/L; Calcium 15 mg/L; Silicate 5 mg/ L; Chloride 40 mg/L; Nitrate 8 mg/L; Carbonate 150 mg/L; pH : 8.2	5200 and 21000	[31]

 doi:10.20944/preprints202506.1740.v1

Several Fe-Mn-based adsorbents tested in synthetic or simulated waters have reported higher breakthrough volumes. For instance, chitosan-coated Fe-Mn binary oxide achieved 3200 BV for As(III) under controlled conditions [25], while the macroporous anion exchanger-supported Fe-Mn binary oxide attained 2300 BV in a simulated water matrix with nitrate, carbonate, and chloride [21]. However, these materials were tested in idealized conditions with minimal competing ions, whereas the Fe-Mn nanocomposite in this study maintained efficient arsenic removal in real groundwater, where competing ions are naturally present.

When assessing adsorption efficiency in real groundwater, the Fe-Mn nanocomposite demonstrated superior performance compared to certain Fe-Mn-based adsorbents. For example, granular activated carbon Fe-Mn binary oxide (GAC-FMBO) exhibited a significantly lower breakthrough volume of 83 BV [13], likely due to strong competition from natural organic matter (NOM), phosphate (1.33 mg/L), and high alkalinity. In contrast, the Fe-Mn nanocomposite exhibited a sevenfold increase in BV (587 BV), confirming its greater resistance to competing ions. Additionally, the HZO@D201 nanocomposite [30], tested under similar groundwater conditions containing 0.1 mg/L As(III) with competing anions, reached 600 BV before breakthrough, a value comparable to the 587 BV obtained in this study, further reinforcing the robust adsorption performance of the Fe-Mn nanocomposite in real-world applications. Moreover, a FMBO-diatomite composite achieved an exceptionally high 7000 BV after 15 regeneration cycles [20], demonstrating strong long-term reusability. However, this system was tested in anaerobic groundwater, which can significantly affect adsorption behavior by reducing competition from oxidized species. In contrast, the FMBO-impregnated nylon 6 fiber (IMBNP-nylon 6) showed 5200 BV and 21000 BV in spiked RO water [31], highlighting its effectiveness under controlled conditions but leaving open questions regarding its performance in real groundwater matrices.

3.2.1. Modelling of Arsenic Adsorption in Fixed-Bed Columns

The data obtained from the fixed-bed column experiments was modelled using three widely applied kinetic models: Thomas, Adams-Bohart, and Yoon-Nelson (Figure 3). These models provide insights into adsorption capacity, rate constants, and breakthrough behaviour under different operational conditions (Table 8).

 doi:10.20944/preprints202506.1740.v1

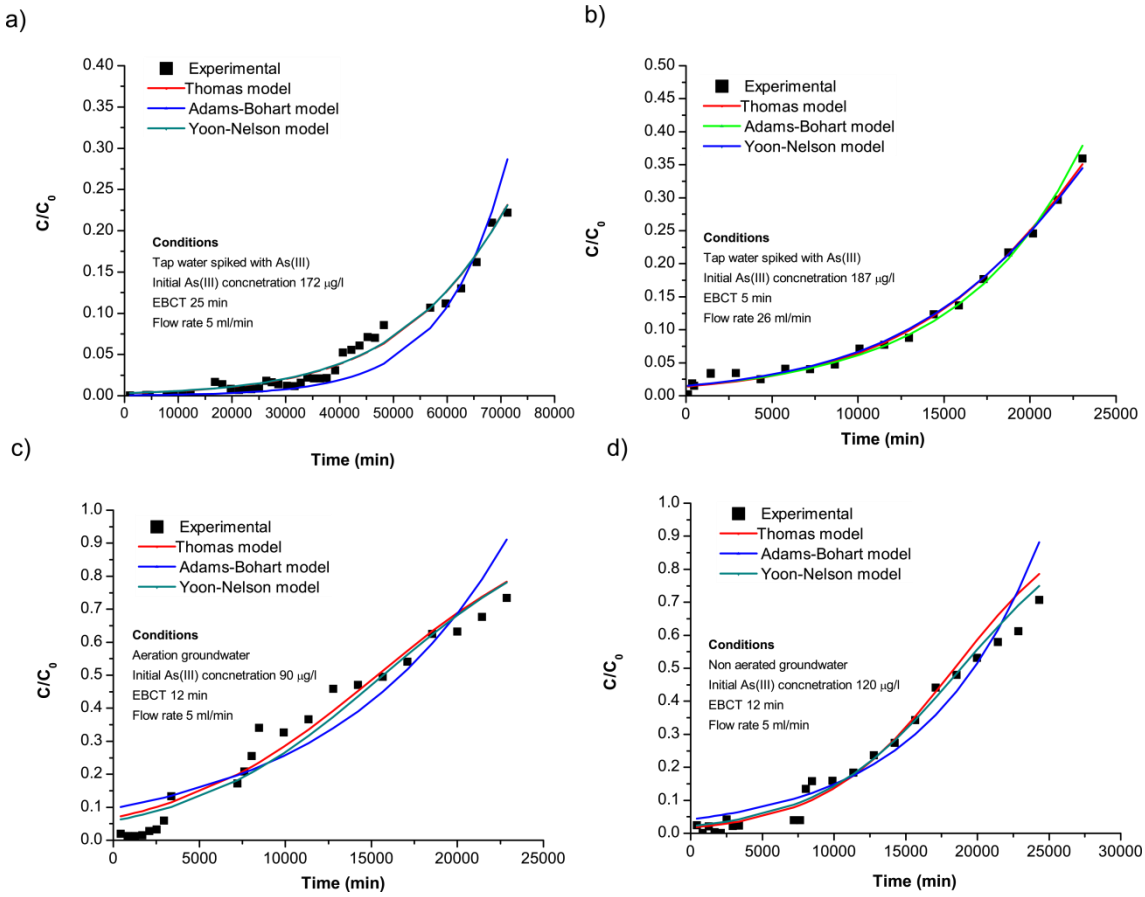

Figure 3. Fitting of nonlinear Thomas, Adams-Bohart and Yoon-Nelson models to the experimental data for the arsenic adsorption in the fixed-bed column studies for the Fe-Mn nanocomposite a) Column I b) Column II c) Column III and d) Column IV.

Table 8. Parameters of the Thomas, Adams-Bohart, and Yoon-Nelson models obtained from modelling experimental data of As(III) adsorption on the Fe-Mn nanocomposite in fixed-bed column studies.

		Thomas constant			**Adams-Bohart**			**Yoon Nelson**		
	q_{exp} (mg/g)	q_t (mg/g)	K_{Th} (L/mg min)	R^2	No (mg/L)	K_{AB} (L/mg min)	R^2	k_{YN} (/min^{-1})	ɪ (min)	R^2
Column I	1.02	1.34	0.0003765	0.9744	588	0.000489	0.9124	0.0000641	90014	0.9915
Column II	1.42	1.71	0.000845	0.9920	863	0.000747	0.9909	0.000153	27248	0.9915
Column III	0.238	0.252	0.00191	0.9824	122	0.00109	0.8754	0.000177	15690	0.9497
Column IV	0.343	0.405	0.00183	0.9760	174	0.00104	0.9384	0.000202	18871	0.9733

All three models—Thomas, Adams-Bohart, and Yoon-Nelson—exhibited high R^2 values (≥ 0.97 for most columns), confirming their suitability for predicting arsenic adsorption and breakthrough behaviour. However, each model describes different aspects of the adsorption process, offering a complementary perspective on the adsorption dynamics. The Thomas model is commonly used to estimate the maximum adsorption capacity (q_t) and is based on the assumption that adsorption follows Langmuir kinetics, with no axial dispersion and mass transfer limitations at the solid-liquid interface. The Adams-Bohart model is particularly useful for describing the initial phase of the breakthrough curve, assuming that adsorption depends on both the adsorbate concentration and the

 doi:10.20944/preprints202506.1740.v1

number of available adsorption sites. The Yoon-Nelson model simplifies the breakthrough curve analysis by estimating the time required for 50% breakthrough of the adsorbate, making it valuable for assessing column exhaustion time [34–36].

Influence of Flow Rate and EBCT on Adsorption Performance. Flow rate and empty bed contact time (EBCT) are critical parameters affecting arsenic removal efficiency in fixed-bed column studies. Column I and Column II, which treated tap water spiked with As(III), operated at different flow rates and EBCTs (25 and 5 min respectively), providing insight into the impact of contact time on adsorption efficiency. The results indicate that Column II exhibited faster adsorption kinetics compared to Column I, as reflected in its higher Thomas rate constant (K_{Th} = 0.000845 L/mg min) compared to Column I (K_{Th} = 0.0003765 L/mg min). This suggests that Column II facilitated a more rapid mass transfer of arsenic onto the Fe-Mn nanocomposite, likely due to the higher flow rate reducing diffusion limitations. Similarly, the Adams-Bohart model supports this observation, as Column II had a higher K_{AB} (0.000747 L/mg min) than Column I (0.000489 L/mg min), indicating that Column II reached equilibrium faster due to a higher adsorption rate. The Yoon-Nelson model further reinforces this trend, with Column II exhibiting a shorter breakthrough time (τ = 27248 min) compared to Column I (τ = 90014 min), demonstrating that Column I retained arsenic for a longer duration, albeit at a slower rate. Although Column I has a lower q_t than Column II, it should be born in mind that it successfully treated more As contaminated water (1750 BV) in comparison with Column II (1600 BV) (Figure 4a and b), such that the longer ECBT is a slower but more economic solution. Yunnen et al. [37] also found that the rate constant (K_{Th}) increases as the flow rate rises, whereas it decreases when the initial arsenic concentration increases. However, the maximum adsorption capacity (q_t) follows the opposite trend, increasing with higher initial arsenic concentrations but decreasing as the flow rate increases. This behavior can be attributed to the strong adsorption driving force created by the concentration gradient between the arsenic ions in solution and those on the adsorbent surface. As a result, the column's performance improves under conditions where a higher initial arsenic concentration is present, allowing for more effective adsorption. Overall, these findings highlight the compromise between faster adsorption kinetics in Column II and the slower but prolonged adsorption process in Column I, emphasizing the need to optimize flow rates and EBCT to balance adsorption efficiency, treated BV, and breakthrough time for practical applications.

 doi:10.20944/preprints202506.1740.v1

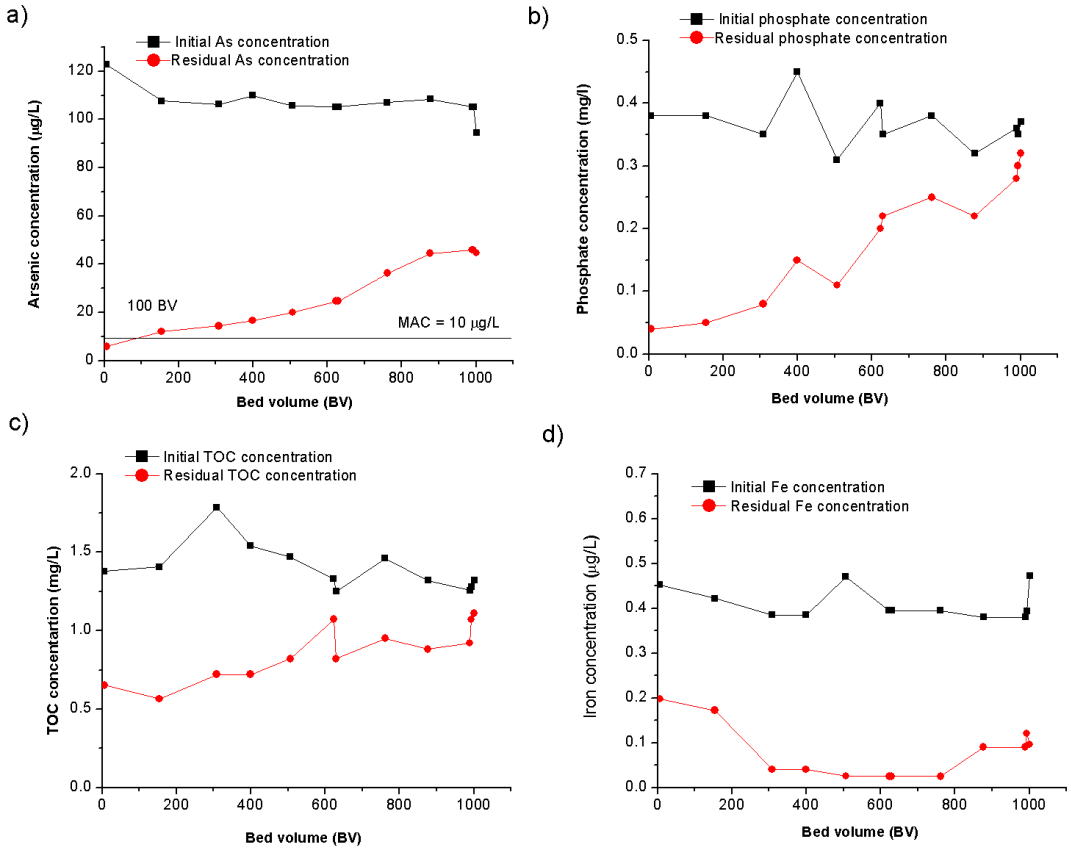

Figure 4. a) Breakthrough curves at Pilot A of a) arsenic; b) phosphate; c) TOC and d) Iron. Initial As concentration 112.07 ± 7.45 µg/L, Phosphate 0.36 ± 0.04 mg/L, TOC 1.4 0± 0.17 mg/L, Fe 0.41± 0.04 mg/L, Flow rate 40 L/h (0.67 L/min), EBCT 5 min.

Impact of Water Matrix on Adsorption Efficiency (Column III and Column IV). The complexity of real groundwater composition was evident in the adsorption behaviour observed in Column III and Column IV, with untreated and aerated groundwater, respectively. The breakthrough curves indicated that arsenic removal was significantly lower in groundwater compared to tap water, with breakthrough occurring at 365 BV in Column III and 587 BV in Column IV. The Thomas model confirmed this trend, showing lower adsorption capacities in groundwater columns (q_t = 0.252 mg/g for Column III and 0.405 mg/g for Column IV), suggesting that competing ions (primarily phosphate) reduced arsenic adsorption efficiency. The higher Thomas rate constant (K_{Th}) in groundwater columns further indicated a faster initial adsorption rate, but due to rapid saturation, arsenic broke through the column earlier. Similarly, the Adams-Bohart model showed higher K_{AB} values in groundwater columns, indicating rapid initial adsorption, but the limited availability of active adsorption sites resulted in early saturation. The Yoon-Nelson model also reflected shorter adsorption half-times (ƭ) in groundwater columns, confirming that the groundwater columns had a considerably shorter operative life than the tap water columns. These findings demonstrate that groundwater chemistry plays a crucial role in determining adsorption efficiency, requiring additional considerations when applying Fe-Mn-based nanocomposites in real-world treatment systems.

Effect of Aeration on Arsenic Removal Efficiency (Column III vs. Column IV). To investigate the impact of aeration as a pre-treatment strategy, the performance of Column III (aerated groundwater) was compared to Column IV (untreated groundwater). The results indicated that aeration did not enhance arsenic adsorption efficiency, as evidenced by the low adsorption capacity (q_t = 0.252 mg/g) observed in Column III. This suggests that removal of Fe(II) through aeration reduced the beneficial effects of arsenic removal by co-precipitation

3.3. Pilot Study

 doi:10.20944/preprints202506.1740.v1

After conducting batch and laboratory-scale column experiments, the performance of the Fe-Mn-based material for arsenic removal from groundwater containing arsenic (Table 1) was evaluated in a pilot study under two different operating conditions. In Pilot A, the system operated at a flow rate of 40 L/h (0.67 L/min), while in Pilot B, the flow rate was 22 L/h (0.367 L/min) (Table 5). Figures 4 and 5 present the breakthrough curves obtained for these different flow rates.

The results presented in **Figure 4a** indicate that the Fe-Mn nanocomposite initially exhibited **high efficiency (95.1%)** in removing arsenic from groundwater. As filtration progressed, the efficiency declined, leading to breakthrough after **100 bed volumes (BV)** of treated water, indicating a progressive saturation of adsorption sites. Beyond this point, a more pronounced decrease was observed, with removal efficiency further reducing to **52.7%** by the end of the experiment. As previously discussed in Section 3.2, this reduced operational lifespan of the Fe-Mn nanocomposite can be attributed to the adsorption site saturation caused by presence of competing anions, particularly phosphate and natural organic matter.

To better understand this effect, the concentrations of these anions were also monitored during the filtration process. Figure 4b illustrates phosphate removal, showing an initial efficiency of 89.47%, which gradually decreased to 13.5% over time. The sharp decline in phosphate removal suggests strong competition between phosphate and arsenic for adsorption sites, which likely contributed to the decreased arsenic removal efficiency. Given that phosphates are known to have a high affinity for iron-based adsorbents, their presence in groundwater significantly impacts the adsorption of arsenic, as observed in previous studies [9,10,14]. Additionally, Figure 4c presents the behaviour of total organic carbon (TOC) removal during filtration. The Fe-Mn nanocomposite initially exhibited a TOC removal efficiency of **59.9%,** which fluctuated but remained relatively high during the early stages of filtration. However, as filtration continued, TOC removal efficiency declined steadily, reaching **15.9%** by the end of the experiment. The reduced removal efficiency suggests that organic matter interacts with the adsorbent, possibly blocking active sites and further decreasing its capacity for arsenic adsorption [38]. Given its elevated concentration in the investigated groundwater (Table 1), iron levels were also monitored during the pilot experiments (Figure 4d). The results indicate that iron removal began at 56.2% in the early filtration phase, with a notable improvement as filtration progressed, reaching 89.6% and peaking at 94.5%. As the experiment continued, iron removal efficiency remained stable at 93.7% for a significant portion of the operation. However, a gradual decline was observed later in the experiment. This suggests that adsorption sites on the Fe-Mn nanocomposite became saturated over time, leading to reduced removal efficiency.

 doi:10.20944/preprints202506.1740.v1

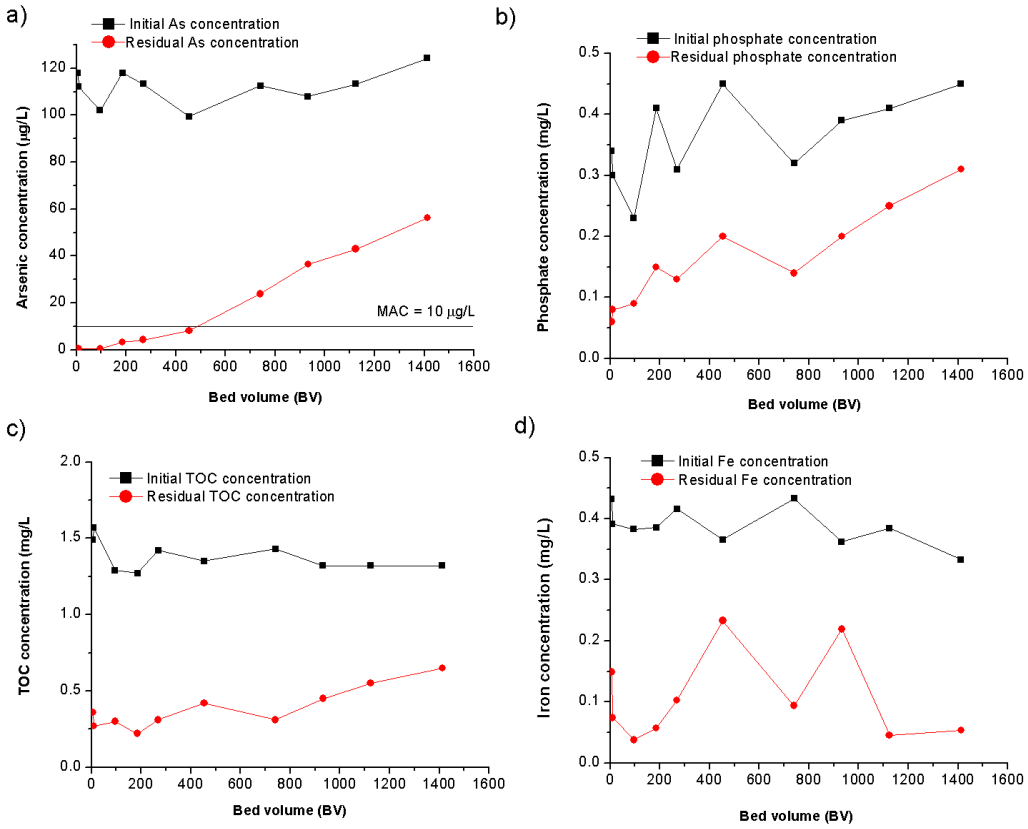

Figure 5. Breakthrough curves at Pilot B for a) Arsenic; b) Phosphate; c) TOC and d) Iron. Initial As concentration 110.72 ± 6.47 µg/L, Phosphate 0.35± 0.07 mg/L, TOC 1.38 ± 0.10 mg/L, Fe 0.39 ± 0.03 mg/L, Flow rate 22 L/h (0.367 L/min), EBCT 15 min.

The results presented in Figure 5a indicate that at a slower filtration rate, the Fe-Mn nanocomposite exhibited prolonged arsenic removal efficiency compared to experiments conducted at higher flow rates. Initially, arsenic removal was highly effective, achieving an efficiency above 99%, which remained stable for an extended duration due to the reduced filtration velocity. This slower flow rate contributed to a delayed breakthrough, occurring at approximately 475 BV, significantly later than in Pilot A, where breakthrough was observed after only 100 BV. The longer empty bed contact time (EBCT) likely enhanced arsenic adsorption by allowing better interaction between the Fe-Mn nanocomposite and the contaminant, thereby extending the operational lifespan of the adsorbent. As adsorption sites gradually became saturated, the arsenic removal efficiency began to decline, dropping to 91.8% during mid-operation and further decreasing to 54.7% by the end of the experiment. This trend is consistent with findings by Chang et al. [20], who investigated arsenic removal from groundwater using Diatomite-FMBO. Their study also observed a significant increase in breakthrough effluent volume with longer EBCT, which was attributed to the limited intra-particle diffusion of the adsorbate into the adsorbent's pores. In their experiments, breakthrough occurred at 180, 450, and 550 BVs for EBCTs of 5, 10, and 20 minutes, respectively.

As shown in Figure 5b, phosphate removal followed a similar trend. The initial efficiency was 82.4%, which gradually decreased over time. Unlike in the previous experiment, where phosphate removal dropped sharply after 500 BV, in this case, the efficiency declined more gradually, reaching 31.1% at the later stages of operation. The extended contact time appeared to mitigate some of the negative competitive adsorption effects, allowing the Fe-Mn nanocomposite to sustain phosphate removal for a longer period. However, despite this improvement, the competition between arsenic and phosphate remained a limiting factor for arsenic removal, reducing the overall adsorption efficiency as filtration progressed. Figure 5c presents TOC removal trends under the slower filtration rate. The initial TOC removal efficiency was 82.8%, fluctuating but remaining relatively high during

 doi:10.20944/preprints202506.1740.v1

the early stages of filtration. As with arsenic and phosphate, TOC removal efficiency gradually decreased over time, dropping to 50.8% at the end of the experiment. The lower filtration velocity allowed for more effective organic matter adsorption, reducing the fouling effects that were more prominent in the higher flow rate experiment. Nonetheless, as filtration continued, TOC still interfered with adsorption, likely blocking active sites and further contributing to the decrease in arsenic removal efficiency. As show in Figure 5d iron removal began at 65.5% and as the experiment continued iron removal efficiency exhibited fluctuations between 39.5% and 88.2%, ultimately reaching 83.9% by the end of the study suggests that adsorption sites on the Fe-Mn nanocomposite became saturated over time.

Compared to the higher filtration rate, Pilot B demonstrated enhanced arsenic removal efficiency and a delayed breakthrough point, confirming that a slower flow rate improves adsorption performance. The longer residence time facilitated better mass transfer and prolonged the Fe-Mn nanocomposite's operational lifespan. However, despite this advantage, the presence of phosphate and TOC still contributed to performance decline, emphasizing the importance of pretreatment strategies to minimize competitive adsorption effects.

3.1.1. Modelling of Arsenic Adsorption Under Realistic Treatment Conditions

To further assess the adsorption capacity of the adsorbent for arsenic removal under realistic conditions and to evaluate its performance across different operational parameters (including varying flow rates, EBCT, and bed height) (Table 8), data from the two pilot-scale investigations were modelled using the Thomas, Adams-Bohart, and Yoon-Nelson models (Figure 6, Table 9). Given that phosphate is recognized as the primary competitor for arsenic, its adsorption capacity on the Fe-Mn nanocomposite was also evaluated.

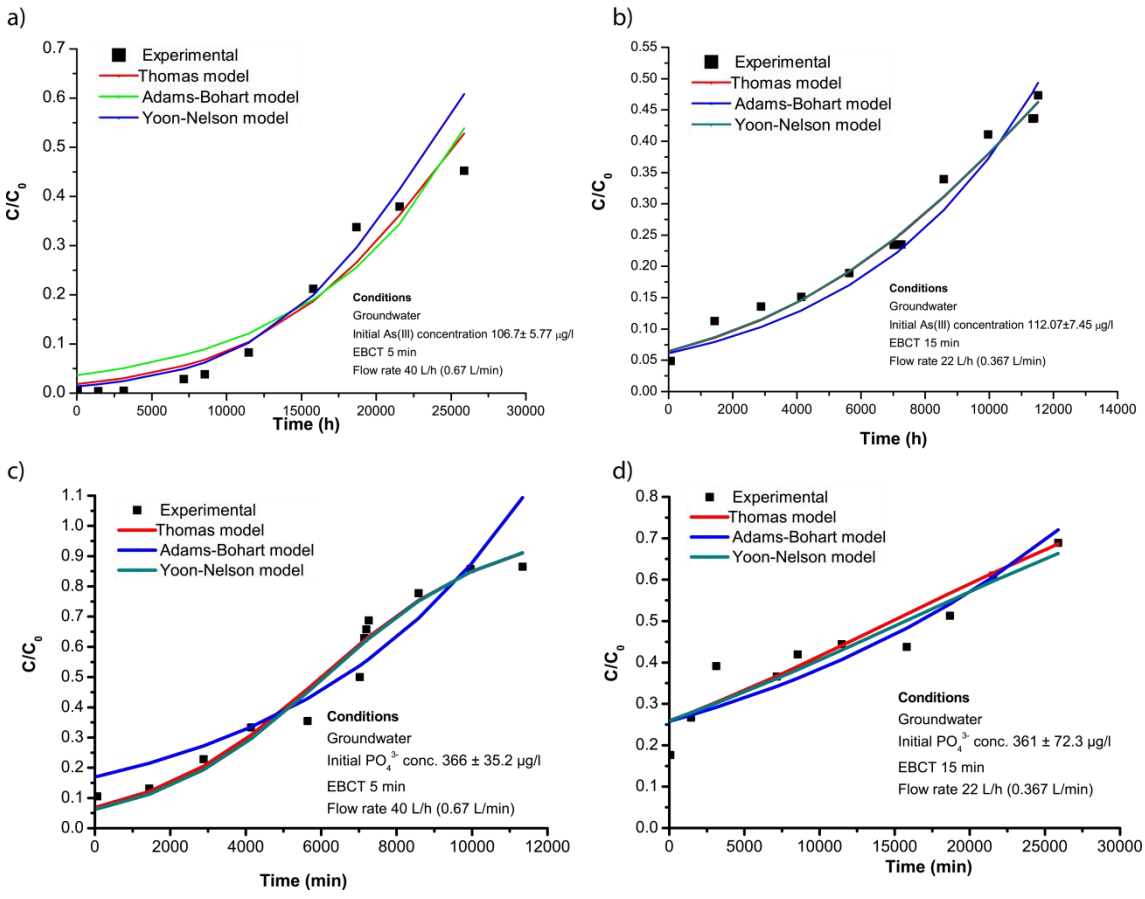

Figure 6. Nonlinear fitting of the Thomas, Adams-Bohart, and Yoon-Nelson models to the data from the pilot: a) Pilot A As removal, b) Pilot B Arsenic removal; c) Pilot A phosphate removal; d) Pilot B phosphate removal.

 doi:10.20944/preprints202506.1740.v1

Table 9. Parameters of the Thomas, Adams-Bohart, and Yoon-Nelson models obtained from modelling experimental data of arsenic and phosphate adsorption on the Fe-Mn nanocomposite pilot studies.

			Thomas constant			**Adams-Bohart**			**Yoon-Nelson**		
		q_{exp} (mg/g)	q_t (mg/g)	K_{Tb} (L/mg min)	R^2	No (mg/L)	K_{AB} (L/mg min)	R^2	K_{YN} (min^{-1})	τ (min)	R^2
Pilot A	Arsenic	0.337	0.551	0.00206	0.9497	327	0.00171	0.9589	0.000218	12197	0.9802
	Phosphate	0.811	0.926	0.00118	0.9726	792	0.000448	0.8598	0.000445	6091	0.9635
Pilot B	Arsenic	0.243	0.417	0.00139	0.9485	216	0.000924	0.9502	0.000181	23463	0.9234
	Phosphate	0.731	0.789	0.000196	0.9864	770	0.000111	0.8818	0.0000667	15719	0.9881

The Thomas model results show that the theoretical capacity (q_t) was higher for arsenic in Pilot A (0.551 mg/g) than in Pilot B (0.417 mg/g) suggesting that higher flow rates enhance the initial adsorption capacity. However, the breakthrough time was significantly longer in Pilot B, as confirmed by the Yoon-Nelson model, which predicted breakthrough times of 23463 min in Pilot B compared to 12197 min in Pilot A. This was consistent with the observed breakthrough volumes of 100 vs 450 BV (Figure 5). This confirms that a lower flow rate and longer EBCT improve operational lifespan, delaying arsenic breakthrough and increasing adsorption stability. as was also observed in the results of the column experiments (Figure 3). The Adams-Bohart model shows that the saturation adsorption capacity (No) for arsenic was 327 mg/L in Pilot A and 216 mg/L in Pilot B, indicating that arsenic uptake was more effective in the higher flow rate system. However, the rate constant (K_{AB}) was higher in Pilot A (0.00171 L/mg min) than in Pilot B (0.000924 L/mg min), reinforcing that higher flow rates lead to faster adsorption kinetics but also faster saturation of the adsorbent (Table 8).

Phosphate is recognized as a strong competitor for arsenic adsorption due to its higher affinity for iron-based adsorbents. The modelling results confirm that phosphate adsorption followed a similar trend to arsenic but with higher overall adsorption capacity. The Thomas model shows that phosphate adsorption capacity was 0.926 mg/g in Pilot A and 0.823 mg/g in Pilot B, significantly higher than the arsenic adsorption. This confirms that phosphate strongly competes for adsorption sites, reducing arsenic removal efficiency wherever it is present [25,39]. The Yoon-Nelson model results indicate that phosphate adsorption lasted longer in Pilot B (7291 min) than in Pilot A (6091 min), further suggesting that a lower flow rate and higher bed volume improve phosphate retention. However, the rate constant (K_{YN}) was higher in Pilot A (0.000445 min^{-1}) than in Pilot B (0.000128 min^{-1}), indicating that phosphate adsorption was faster under higher flow conditions but less sustainable over time. The Adams-Bohart model also supports this trend, showing that the adsorption capacity coefficient (No) for phosphate was much higher than for arsenic (792 mg/L in Pilot A and 761 mg/L in Pilot B). However, the rate constant (K_{AB}) for phosphate was significantly lower than for arsenic, confirming slower initial adsorption kinetics despite the higher overall capacity. The competition between phosphate and arsenic is further evident from the greater phosphate adsorption capacities in both Pilots. In Pilot B, where phosphate adsorption lasted longer, arsenic removal efficiency was lower, suggesting that phosphate outcompetes arsenic at a lower flow rate and higher bed height (Table 8). These findings suggest that optimizing operational parameters—such as flow rate, EBCT, and potentially, a pre-treatment for phosphate removal, can significantly enhance arsenic removal efficiency in real-world applications and prolong the lifespan of the adsorbent.

3.4. Comparison Between Batch Experiments and Pilot-Scale Studies

 doi:10.20944/preprints202506.1740.v1

To evaluate whether a correlation exists between batch adsorption experiments, fixed-bed column studies, and pilot-scale investigations, adsorption capacities were compared across the different scales while focusing only on real groundwater conditions (Table 10). The batch adsorption experiments, modelled using the Langmuir isotherm, predicted a maximum adsorption capacity (q_{max}) of 4.71 mg/g for arsenic-contaminated groundwater. In contrast, adsorption capacities obtained from the Thomas model in fixed-bed column studies were 0.252 mg/g in Column III (aerated groundwater) and 0.405 mg/g in Column IV (non aerated groundwater). In the pilot-scale study, the adsorption capacities ranged from 0.551 mg/g in Pilot A to 0.417 mg/g in Pilot B.

Table 10. Comparison of adsorption capacity of Fe-Mn nanocomposite obtained in different scales, from batch to pilot.

Scale	mass adsorbent		q_{exp} (mg/g)	q (Langmuir or Thomas model) (mg/g)	Breakthrough point
Batch experiments	20	mg		4.71	
Column III	28	g	0.238	0.252	587
Column IV	28	g	0.343	0.405	365
Pilot A	1.6	kg	0.337	0.551	100
Pilot B	2.5	kg	0.243	0.417	475

The modelled adsorption capacity in batch experiments was significantly higher than in column and pilot studies which was expected since batch systems provide sufficient equilibrium time and significantly higher theoretical maximum loads, allowing the adsorbent to reach its maximum adsorption potential. In contrast, flow-through systems operate under dynamic conditions, where adsorption efficiency is influenced by flow rate, EBCT and competitive adsorption effects. Among the fixed-bed column experiments and pilot-scale adsorption studies, Column III, Column IV, and Pilot B share similar EBCT values (~15 min), which contributes to their comparable adsorption performance. Notably, the adsorption capacity in Pilot B (0.243 mg/g) closely aligns with Column IV (0.238 mg/g), indicating a strong correlation between fixed-bed column experiments and pilot-scale adsorption studies. Additionally, the breakthrough point for Pilot B (475 BV) is similar to Column IV (587 BV), further supporting this relationship.

The impact of flow rate, EBCT, and bed depth is evident when comparing adsorption behaviour across different setups. Pilot A, which had a shorter EBCT (~5 min), exhibited lower arsenic adsorption and an earlier breakthrough (100 BV), confirming that shorter contact time reduces adsorption efficiency. Meanwhile, the longer EBCT in Pilot B (15 min) resulted in extended adsorption performance, similar to what was observed in Column III and IV. Additionally, the greater bed height in the pilot-scale study compared to the column experiments likely contributed to prolonged breakthrough times.

Overall, these findings highlight the importance of continuous-flow experiments in assessing the performance of new adsorbents. The investigations using real groundwater samples confirmed that the batch experiments tend to overestimate adsorption capacity, whereas fixed-bed column studies provide more reliable predictions for pilot-scale adsorption performance. The strong agreement between Column IV and Pilot B suggests that well-designed fixed-bed column studies can effectively simulate significantly larger real-world pilot-scale conditions, although it should be noted that even the column experiments in this work are about an order of magnitude larger than many reported in the literature. The results from the experiments using raw groundwater emphasize the need to optimize operational parameters and implement pre-treatment strategies for competing anions to enhance arsenic removal efficiency in large-scale applications, as well as the benefits of optimising adsorbents for more selective arsenic removal especially over phosphate [40].

 doi:10.20944/preprints202506.1740.v1

4. Conclusions

This study provides a comprehensive evaluation of a Fe-Mn-based nanocomposite for arsenic removal from groundwater across batch, fixed-bed column, and pilot-scale experiments. Adsorbent masses in these three experiment types were in the mg, g and kg ranges. The adsorption capacity observed in batch experiments (qmax = 6.25 mg/g in synthetic water, 4.71 mg/g in real groundwater) was significantly higher than in the continuous-flow conditions, where operational constraints and competing anions influenced performance. In fixed-bed columns, the adsorption capacity was 0.405 mg/g, whereas in pilot-scale tests, it reached 0.551 mg/g, highlighting the challenges of translating equilibrium-based batch findings to dynamic operational environments. Breakthrough curve analysis demonstrated that pilot-scale results closely aligned with fixed-bed column studies, reinforcing the necessity of well-designed column experiments to predict real-world performance. The influence of phosphate as a key competing anion was confirmed, with phosphate adsorption capacity (0.926 mg/g) exceeding that of arsenic (0.417 mg/g) in the pilot scale, necessitating the development of pre-treatment strategies to enhance arsenic removal efficiency. Additionally, kinetic modelling using Thomas, Adams-Bohart, and Yoon-Nelson models provided valuable insights into the adsorption mechanisms, indicating that lower flow rates and extended EBCT significantly enhance arsenic retention and improve operational stability. This study highlights the critical role of continuous-flow experiments in evaluating adsorbent performance, demonstrating that batch studies often overestimate adsorption capacity. The findings underscore the importance of optimizing flow conditions, EBCT, and competing ion management to enhance the efficiency and longevity of Fe-Mn-based adsorbents in practical applications. By integrating laboratory-scale column testing with pilot-scale evaluations, this research demonstrates how to bridge the gap between theoretical and real-world performance, paving the way for larger-scale implementations of Fe-Mn nanocomposites as sustainable, high-efficiency adsorbents for arsenic removal in drinking water treatment

Supplementary Materials: The following supporting information can be downloaded at the website of this paper posted on Preprints.org, Figure S1. Correlation between q_{max} values reported in the literature and the maximum initial concentrations of the experimental isotherms. Table S1. Operational conditions at lab scale column experiment. Table S2. Residual concentrations of Fe and Mn in water after treatment with the Fe-Mn nanocomposite.

Author Contributions: Conceptualization, Jasmina Nikić, Malcolm Watson and Jasmina Agbaba; Formal analysis, Jasmina Nikić, Jovana Jokić Govedarica, Malcolm Watson, Đorđe Pejin and Aleksandra Tubić; Funding acquisition, Jasmina Agbaba; Investigation, Jasmina Nikić, Jovana Jokić Govedarica, Malcolm Watson, Đorđe Pejin and Jasmina Agbaba; Visualization, Jovana Jokić Govedarica; Writing – original draft, Jasmina Nikić; Writing – review & editing, Jasmina Nikić, Malcolm Watson and Jasmina Agbaba.

Funding: This research was supported by the Science Fund of the Republic of Serbia, Grant No. 4858, Scale-up of bifunctional Fe–Mn binary oxide nanocomposite filter media: an innovative approach for water purification-NanoCompAs. Funding acquired by JA.

Data Availability Statement: The raw data supporting the conclusions of this article will be made available by the authors on request.

Conflicts of Interest: The authors declare no conflicts of interest. The funders had no role in the design of the study; in the collection, analyses, or interpretation of data; in the writing of the manuscript; or in the decision to publish the results.

References

1. Shaji, E.; Santosh, M.; Sarath, K.V.; et al. Arsenic contamination of groundwater: A global synopsis with focus on the Indian Peninsula. *Geosci. Front.* **2021**, *12*, 101079. https://doi.org/10.1016/j.gsf.2020.08.015

 doi:10.20944/preprints202506.1740.v1

2. Guo, J.; Cao, W.; Lang, G.; et al. Worldwide Distribution, Health Risk, Treatment Technology, and Development Tendency of Geogenic High-Arsenic Groundwater. *Water* **2024**, *16*, 1–25. https://doi.org/10.3390/w16030478
3. Mukherjee, A.; Coomar, P.; Sarkar, S.; et al. Arsenic and other geogenic contaminants in global groundwater. *Nat. Rev. Earth Environ.* **2024**, *5*, 312–328. https://doi.org/10.1038/s43017-024-00519-z
4. Fatoki, J.O.; Badmus, J.A. Arsenic as an environmental and human health antagonist: A review of its toxicity and disease initiation. *J. Hazard. Mater. Adv.* **2022**, *5*, 100052. https://doi.org/10.1016/j.hazadv.2022.100052
5. Patel, B.; Gundaliya, R.; Desai, B.; et al. Groundwater arsenic contamination: impacts on human health and agriculture, ex situ treatment techniques and alleviation. *Environ. Geochem. Health* **2023**, *45*, 1331–1358. https://doi.org/10.1007/s10653-022-01334-5
6. Yang, Y.; Mo, W.; Wei, C.; et al. Fe/Mn-MOF-driven rapid arsenic decontamination: Mechanistic elucidation of adsorption processes and performance optimization. *J. Water Process Eng.* **2025**, *69*, 106691. https://doi.org/10.1016/j.jwpe.2024.106691
7. Lin, L.; Song, Z.; Liu, X.; et al. Arsenic volatilization in flooded paddy soil by the addition of Fe-Mn-modified biochar composites. *Sci. Total Environ.* **2019**, *674*, 327–335. https://doi.org/10.1016/j.scitotenv.2019.04.144
8. Zhang, M.; Ma, X.; Li, J.; et al. Enhanced removal of As(III) and As(V) from aqueous solution using ionic liquid-modified magnetic graphene oxide. *Chemosphere* **2019**, *234*, 196–203. https://doi.org/10.1016/j.chemosphere.2019.06.057
9. Shan, H.; Mo, H.; Liu, Y.; et al. As(III) removal by a recyclable granular adsorbent through doping Fe-Mn binary oxides into graphene oxide chitosan. *Int. J. Biol. Macromol.* **2023**, *237*, 124184. https://doi.org/10.1016/j.ijbiomac.2023.124184
10. Lv, C.; Li, Z.; Ding, J.; et al. Arsenate adsorption, desorption, and re-adsorption on Fe–Mn binary oxides: Impact of co-existing ions. *Desalin. Water Treat.* **2024**, *320*, 100678. https://doi.org/10.1016/j.dwt.2024.100678
11. Nikić, J.; Watson, M.; Jokić Govedarica, J.; et al. Adsorption Performance of Fe–Mn Polymer Nanocomposites for Arsenic Removal: Insights from Kinetic and Isotherm Models. *Materials* **2024**, *17*, 1–21. https://doi.org/10.3390/ma17205089
12. Ryu, S.; Jeon, E.; Yang, J.S.; Baek, K. Adsorption of As(III) and As(V) in groundwater by Fe–Mn binary oxide-impregnated granular activated carbon (IMIGAC). *J. Taiwan Inst. Chem. Eng.* **2017**, *72*, 62–69. https://doi.org/10.1016/j.jtice.2017.01.004
13. Nikić, J.; Agbaba, J.; Watson, M.A.; et al. Arsenic adsorption on Fe–Mn modified granular activated carbon (GAC–FeMn): batch and fixed-bed column studies. *J. Environ. Sci. Health A* **2019a**, *54*, 168–178. https://doi.org/10.1080/10934529.2018.1541375
14. Nikić, J.; Watson, M.; Tenodi, K.Z.; et al. Pilot study on arsenic removal from phosphate rich groundwater by in-line co-agulation and adsorption. *J. Hazard. Mater. Adv.* **2023**, *10*, 100280. https://doi.org/10.1016/j.hazadv.2023.100280
15. Ghosh, A.; Chakrabarti, S.; Ghosh, U.D.C. Fixed-bed column performance of Mn-incorporated iron(III) oxide nanoparticle agglomerates on As(III) removal from the spiked groundwater in lab bench scale. *Chem. Eng. J.* **2014**, *248*, 18–26. https://doi.org/10.1016/j.cej.2014.03.010
16. Malbenia John, M.; Benettayeb, A.; Belkacem, M.; et al. An overview on the key advantages and limitations of batch and dynamic modes of biosorption of metal ions. *Chemosphere* **2024**, *357*, 142051. https://doi.org/10.1016/j.chemosphere.2024.142051
17. Carneiro, M.A.; Pintor, A.M.A.; Boaventura, R.A.R.; et al. Arsenic and antimony desorption in water treatment processes: Scaling up challenges with emerging adsorbents. *Sci. Total Environ.* **2024**, *929*, 172602. https://doi.org/10.1016/j.scitotenv.2024.172602
18. Zhang, G.S.; Qu, J.H.; Liu, H.J.; et al. Removal mechanism of As(III) by a novel Fe-Mn binary oxide adsorbent: Oxidation and sorption. *Environ. Sci. Technol.* **2007**, *41*, 4613–4619. https://doi.org/10.1021/es063010u

 doi:10.20944/preprints202506.1740.v1

19. Nikić, J.; Watson, M.; Tubić, A.; et al. Arsenic removal from water using a one-pot synthesized low-cost mesoporous Fe–Mn-modified biosorbent. *J. Serb. Chem. Soc.* **2019b**, *84*, 327–342. https://doi.org/10.2298/JSC180809099N
20. Chang, F.; Qu, J.; Liu, H.; et al. Fe-Mn binary oxide incorporated into diatomite as an adsorbent for arsenite removal: Preparation and evaluation. *J. Colloid Interface Sci.* **2009**, *338*, 353–358. https://doi.org/10.1016/j.jcis.2009.06.049
21. Li, X.; He, K.; Pan, B.; et al. Efficient As(III) removal by macroporous anion exchanger-supported Fe-Mn binary oxide: Behavior and mechanism. *Chem. Eng. J.* **2012**, *193–194*, 131–138. https://doi.org/10.1016/j.cej.2012.04.036
22. Xu, F.; Chen, H.; Dai, Y.; et al. Arsenic adsorption and removal by a new starch stabilized ferromanganese binary oxide in water. *J. Environ. Manage.* **2019**, *245*, 160–167. https://doi.org/10.1016/j.jenvman.2019.05.071
23. Kong, S.; Wang, Y.; Hu, Q.; et al. Magnetic nanoscale Fe-Mn binary oxides loaded zeolite for arsenic removal from synthetic groundwater. *Colloids Surf. A Physicochem. Eng. Asp.* **2014**, *457*, 220–227. https://doi.org/10.1016/j.colsurfa.2014.05.066
24. Lin, L.; Qiu, W.; Wang, D.; et al. Arsenic removal in aqueous solution by a novel Fe-Mn modified biochar composite: Characterization and mechanism. *Ecotoxicol. Environ. Saf.* **2017**, *144*, 514–521. https://doi.org/10.1016/j.ecoenv.2017.06.063
25. Qi, J.; Zhang, G.; Li, H. Efficient removal of arsenic from water using a granular adsorbent: Fe-Mn binary oxide impregnated chitosan bead. *Bioresour. Technol.* **2015**, *193*, 243–249. https://doi.org/10.1016/j.biortech.2015.06.102
26. Nikić, J.; Watson, M.A.; Isakovski, M.K.; et al. Synthesis, characterization and application of magnetic nanoparticles modified with Fe-Mn binary oxide for enhanced removal of As(III) and As(V). *Environ. Technol.* **2019c**, *0*, 1–30. https://doi.org/10.1080/09593330.2019.1705919
27. Wang, Y.; Gao, Y.; Zhu, Z.; et al. Enhanced Arsenic Removal from Aqueous Solution by Fe/Mn-C Layered Double Hydroxide Composite. *Adsorpt. Sci. Technol.* **2021**, *2021*, 1–12. https://doi.org/10.1155/2021/8891643
28. Roy, P.; Mondal, N.K.; Bhattacharya, S.; et al. Removal of arsenic(III) and arsenic(V) on chemically modified low-cost adsorbent: batch and column operations. *Appl. Water Sci.* **2013**, *3*, 293–309. https://doi.org/10.1007/s13201-013-0082-5
29. Panda, A.P.; Jha, U.; Kumar, S.A.; Swain, S.K. A Simplified and Affordable Arsenic Filter to Prevent Arsenic Poisoning: Lab-Scale Study and Pilot Experiment. *ACS ES&T Water* **2023**, *3*, 4092–4102. https://doi.org/10.1021/acsestwater.3c00475
30. Pan, B.; Li, Z.; Zhang, Y.; et al. Acid and organic resistant nano-hydrated zirconium oxide (HZO)/polystyrene hybrid adsorbent for arsenic removal from water. *Chem. Eng. J.* **2014**, *248*, 290–296. https://doi.org/10.1016/j.cej.2014.02.093
31. Awasthi, V.D.; Yamamura, G.; Kobayashi, A.; et al. Enhanced impregnation of iron manganese binary oxide nanoparticles on nylon 6 fibre for rapid and continuous arsenic [As(III)] removal from drinking water. *J. Water Process Eng.* **2024**, *64*, 105656. https://doi.org/10.1016/j.jwpe.2024.105656
32. Chang, F.; Qu, J.; Liu, R.; et al. Practical performance and its efficiency of arsenic removal from groundwater using Fe-Mn binary oxide. *J. Environ. Sci.* **2010**, *22*, 1–6. https://doi.org/10.1016/S1001-0742(09)60067-X
33. Asif, Z.; Chen, Z. Removal of arsenic from drinking water using rice husk. *Appl. Water Sci.* **2017**, *7*, 1449–1458. https://doi.org/10.1007/s13201-015-0323-x
34. Brion-Roby, R.; Gagnon, J.; Deschênes, J.S.; et al. Investigation of fixed bed adsorption column operation parameters using a chitosan material for treatment of arsenate contaminated water. *J. Environ. Chem. Eng.* **2018**, *6*, 505–511. https://doi.org/10.1016/j.jece.2017.12.032
35. Patel, H. Fixed-bed column adsorption study: a comprehensive review. *Appl. Water Sci.* **2019**, *9*, 45. https://doi.org/10.1007/s13201-019-0927-7
36. Apiratikul, R.; Chu, K.H. Improved fixed bed models for correlating asymmetric adsorption breakthrough curves. *J. Water Process Eng.* **2021**, *40*, 101810. https://doi.org/10.1016/j.jwpe.2020.101810
37. Yunnen, C.; Ye, W.; Chen, L.; et al. Continuous fixed-bed column study and adsorption modeling: Removal of arsenate and arsenite in aqueous solution by organic modified spent grains. *Pol. J. Environ. Stud.* **2017**, *26*, 1847–1854. https://doi.org/10.15244/pjoes/68869

 doi:10.20944/preprints202506.1740.v1

38. Watson, M.; Nikić, J.; Tubić, A.; et al. Repurposing spent filter sand from iron and manganese removal systems as an adsorbent for treating arsenic contaminated drinking water. *J. Environ. Manage.* **2022**, *302*, 114115. https://doi.org/10.1016/j.jenvman.2021.114115
39. Marzi, M.; Towfighi, H.; Shahbazi, K.; et al. Study of arsenic adsorption in calcareous soils: Competitive effect of phosphate, citrate, oxalate, humic acid and fulvic acid. *J. Environ. Manage.* **2022**, *318*, 115532. https://doi.org/10.1016/j.jenvman.2022.115532
40. Weerasundara, L.; Ok, Y.S.; Bundschuh, J. Selective removal of arsenic in water: A critical review. *Environ. Pollut.* **2021**, *268B*, 115668. https://doi.org/10.1016/j.envpol.2020.115668